

APPLICATION OF A CAMERA ARRAY FOR THE UPGRADE OF THE AWAKE SPECTROMETER

Eugenio Senes*¹, F. Pannell², D.A. Cooke², S. Mazzoni¹,
M. Turner¹, M. Wing², G. Zevi Della Porta^{1,3}
¹ CERN, Geneva, Switzerland

² University College London, London, United Kingdom

³ Max Planck Institute for Physics, Munich, Germany

Abstract

The first run of the AWAKE experiment successfully demonstrated the acceleration of an electron beam in the plasma wakefields of a relativistic proton beam. The planned second run will focus on the control of the emittance of accelerated electrons, requiring an upgrade of the existing spectrometer. Preliminary measurements showed that this might be achieved by improving the resolution of the scintillator and with a new design of the optical system. This contribution discusses the application of a digital camera array in close proximity of the spectrometer scintillator, to enable the accelerated electron beam emittance measurement.

INTRODUCTION

In the AWAKE experiment, a 19 MeV electron bunch gets accelerated in the wakefield of a rubidium plasma [1]. The plasma wake is driven by a 400 GeV proton bunch produced in the CERN Super Proton Synchrotron.

In order to measure the characteristics of the accelerated electron beam, a magnetic spectrometer was installed downstream of the plasma cell. The development of the magnetic spectrometer is reported in [2–4].

The core functions of the electron spectrometer are to measure on the accelerated electron beam:

1. The beam peak energy and energy profile
2. The beam charge
3. The beam emittance

In AWAKE Run 1 the resolution proved to be too limited to measure the beam emittance; a study was launched to improve the spectrometer system for AWAKE Run 2. This paper discusses possible technical implementations to improve the spectrometer resolution, focusing on a high resolution optical system. Possible modifications of the spectrometer magnetic lattice to transport the accelerated beam will be discussed elsewhere, and go beyond the scope of this work.

SPECTROMETER DESIGN

Beamline Components

The magnetic components of the spectrometer have not changed since AWAKE Run 1 [5, 6]. The electron and proton

beams exit the plasma, pass through a quadrupole doublet and then through a dipole magnet. A dipole field up to 1.5 T separates the electron and proton beams, introducing a spatial dependence for the electron beam energy in the range 30 MeV–8.5 GeV. After the dipole, the accelerated electrons traverse a 2 mm thick vacuum window, and impact on a 1 m-long plastic scintillator. The scintillator currently in use is a 0.5 mm thick DRZ-High, a terbium-doped, gadolinium oxysulfide ($Gd_2O_2S:Tb$) screen produced by Mitsubishi Chemical. The particle transport through the spectrometer was simulated and validated through measurements with partially stripped ions [7, 8]. A layout of the spectrometer system is shown in Fig. 1.

Optical System

Information on the electron beam structure is reconstructed from the emitted light pattern produced by the scintillator. An accurate imaging of the scintillator emission is essential for a correct measurement of the electron beam parameters.

During AWAKE Run 1, the scintillation light was propagated through a 17 m-long optical line, to reach an intensified camera in a dedicated dark room outside the high radiation area [9, 10]. The camera is equipped with a 400 mm photographic lens, in order to resolve the whole scintillator. Although this system worked, the optical resolution proved to be too limited for emittance measurements.

Recent developments in the CMOS camera infrastructure for AWAKE allowed for placing cameras inside the experimental hall. A camera array was installed within 1.5 m of the scintillator, to record its light. This system is described in detail later on.

Beam Charge Measurement

In order to measure the total accelerated charge, the scintillator light yield is calibrated against a known electron charge. In the past, the calibration was performed by installing the scintillator and the camera in the CLEAR test accelerator [11], and using electron beams with known charge. To allow for the in-situ calibration, a commercial Integrating Current Transformer (ICT) from Bergoz [12] was installed in the beamline upstream of the dipole. The charge signal is detected with custom electronics within a range of 750 pC.

* eugenio.senes@cern.ch

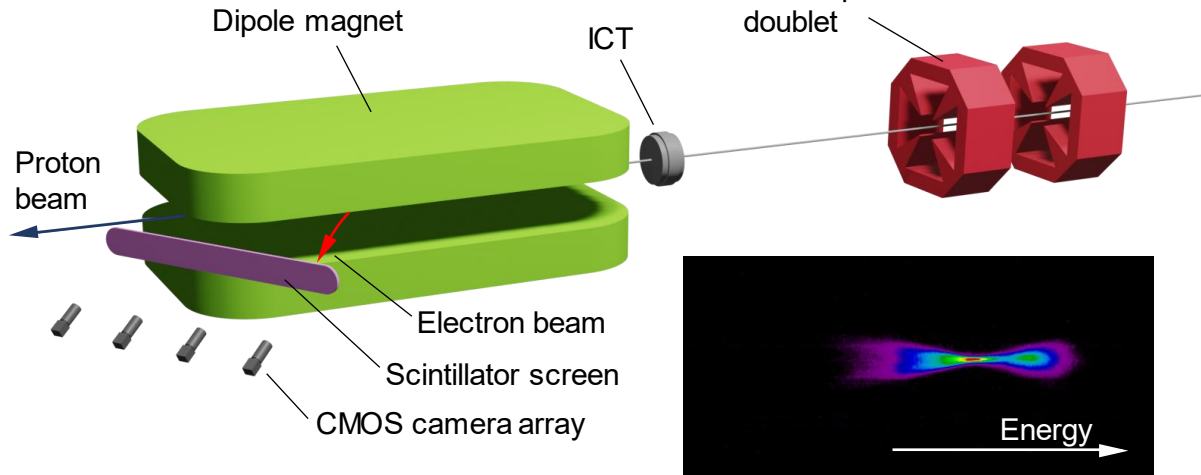


Figure 1: Layout of the spectrometer system in AWAKE. The inset shows a sample image of an accelerated beam from one of the cameras in the array.

DIGITAL CAMERA SYSTEM

Digital Camera Array

A general description of the digital camera infrastructure for AWAKE was given in Ref. [13]. The measurements shown in this work are performed with Basler acA1920-40gm cameras. The camera specifications are shown in Table 1. These devices showed a good resistance to modest radiation environments, and are remotely powered, allowing for reboot to recover from single event upset failures. The cameras are hardware triggered with a 750 μ s delay, to capture the decay of the scintillation light. As the light emission is peaked at 545 nm, each camera is equipped with a 525 ± 46 nm bandpass filter to reduce the background.

A resolution in the order of 100 μ m can be reached with sufficient camera magnification. This is a tradeoff between the distance to the scintillator and the objective focal length. The limitation, arising from high magnification, is that each camera can image only a part of the spectrometer. A camera array is set up to allow the imaging of a larger area of the spectrometer. The larger spectrometer image is then reconstructed by combining the camera images. The recombination algorithm is described later on. The camera array is placed within 1.5 m from the scintillator, with an angle of 30° below the beam plane. This allows both for removing the cameras from the beam plane, where the radiation is higher, and for leaving free space in the optical line towards the intensified camera.

The selected camera lenses are Fujinon HF75HA1S with a focal length of 75 mm and an aperture of f/2.8. The camera array was placed at 110 cm from the scintillator, that is the minimum focusing distance of the lenses. The setup was reproduced in the lab, where USAF1951 targets were used to measure the point spread function (PSF) and hence infer the resolution. Additionally, a different camera model (Basler acA2040-35gm) was tested, featuring smaller pixel size and smaller sensor format. Both cameras showed that

Table 1: Comparison of parameters for the tested cameras. The top half shows camera specifications. The bottom half shows the measured resolution with 75 mm lens at 110 cm distance from the target.

Model		acA1920-40gm	acA2040-35gm
Resolution	[px]	1920 × 1200	2048 × 1536
Pixel size	[μ m]	5.86 × 5.86	3.45 × 3.45
Sensor format		1/1.2"	1/1.8"
Lens		HF75HA1S - 75 mm f/2.8	
Magnification		0.076	
Field of view	[cm]	14.9	9.5
Pixel object size	[μ m]	77	45
PSF σ	[μ m]	77	48

the resolution is dominated by the pixel size of the camera, and that optical resolutions as low as 77 and 48 μ m are reachable at 110 cm distance, respectively. The camera parameters and resolutions are reported in Table 1. These tests showed that high resolution can be achieved at the expense of the field of view. To resolve the full 1 m-long scintillator, the array would require 7 and 11 cameras, respectively. Additionally, the use of sensors with smaller pixel size allows for increasing the distance to the scintillator, reducing the radiation damage.

Camera Calibration

Camera calibration is an essential part of understanding the three-dimensional aspects of objects from two-dimensional images. Extracting metric information from the 2D images acquired by the AWAKE spectrometer camera array forms the basis of the accelerated electron bunch analysis.

The mapping of a 3D point \mathbf{X} in the real-world, to a 2D pixel coordinate, \mathbf{x} , can be described via Eq. (1):

Content from this work may be used under the terms of the CC-BY-4.0 licence (© 2023). Any distribution of this work must maintain attribution to the author(s), title of the work, publisher, and DOI

$$\mathbf{x} = \mathbf{P}\mathbf{X} \quad (1)$$

where \mathbf{P} is the projection matrix – a combination of the intrinsic camera calibration parameters and extrinsic camera parameters of position and orientation.

The process of camera calibration in this work employs Zhang’s method, where the camera observes a planar pattern at different translations, rotations and tilts [14]. This technique offers a simplified, easily reproducible calibration procedure compared to the multiple, orthogonal planes used in 3D reference object-based calibration methods.

The procedure begins by mounting a pattern of known structure and size, in this case a chessboard, on a flat surface. The camera is fixed and the chessboard is imaged at different orientations. The OpenCV-Python [15] library is used and, for every image, a coordinate system is defined in which the chessboard forms the XY plane; all points lying on the chessboard have $Z = 0$. With this approach, the mapping between coordinate systems is simplified as the last column of the rotation matrix within \mathbf{P} can be eliminated.

The corners of the chessboard pattern are located as key points through a function based on the Harris corner detection algorithm [16]. With each point representing an equation in the coordinate mapping system, the camera calibration parameters are obtained from the homography of real-world points to image points. Figure 2 shows the chessboard calibration target repeatedly imaged through one camera on the spectrometer array, with the corners successfully identified.

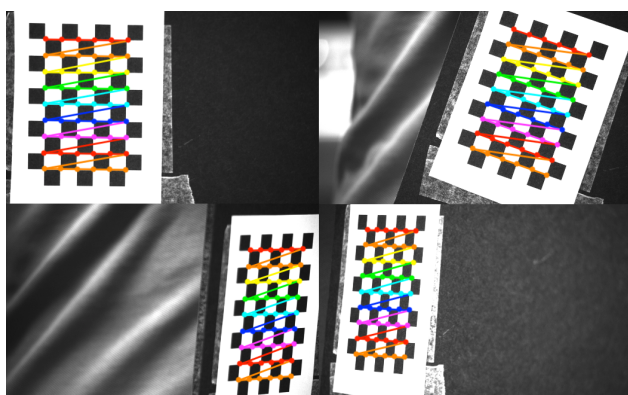


Figure 2: Chessboard calibration pattern captured at different positions and orientations. The corners are located with OpenCV.

Lens distortion effects, such as the ones illustrated in Fig. 3, arise from the lens optical design. The calculation of the camera matrix, distortion coefficients, translation and rotation vectors in the camera calibration procedure allows for the compensation of this effect.

Perspective Correction

As described earlier, the camera array views the spectrometer scintillator screen from an angle of 30° below the beam plane. Whilst it has practical advantages, this setup

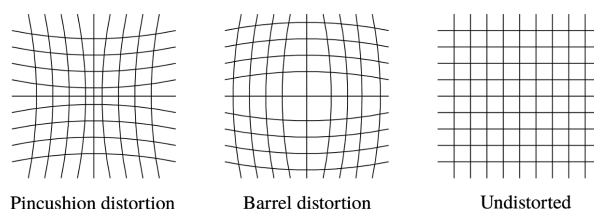


Figure 3: Examples of radial lens distortion, where light rays deviate from rectilinear projection.

introduces a perspective distortion to the acquired images. By looking up at the screen, a foreshortening effect is created, where shapes higher up in the image appear condensed compared to shapes of the same size at the bottom.

Figure 4 demonstrates this effect. The left figure shows an uncorrected USAF1951 resolution target viewed through a spectrometer camera. The right figure is the same image but corrected for the perspective distortion. In addition to the rectified scaling offered by the perspective correction, as evidenced by the lengthened bars and increased target height, the image is rotated to create a ‘head on’ view of the target. The perspective correction was achieved by mapping the coordinates of the target corners in the unprocessed image to the corresponding corners in a scale, technical drawing of the same target.

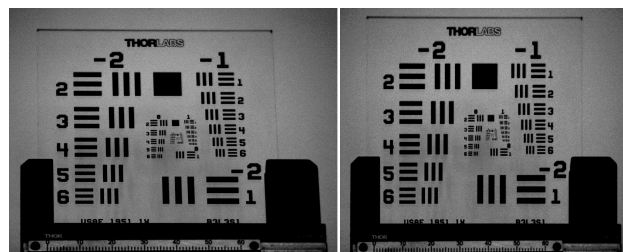


Figure 4: USAF1951 resolution target as seen from an unprocessed spectrometer image 30° below the beam plane (left) and a perspective corrected image to view ‘head on’ (right).

Emittance measurements with the camera array involve extracting the transverse size of the electron beam waist. Without perspective correction, the measured beam size will differ from reality, impacting the validity of emittance results. It is therefore essential to apply the appropriate perspective correction prior to analysis.

To correct the scintillator screen for perspective distortion, a screen target with commensurate dimensions with the scintillator is temporarily placed across the screen and imaged by all cameras in the array. Similarly to the resolution target perspective correction, key coordinates from the acquired images are mapped to the equivalent features in a technical drawing of the screen target. This can be seen in Fig. 5, where corrected images are sampled up to the same size of the drawing.

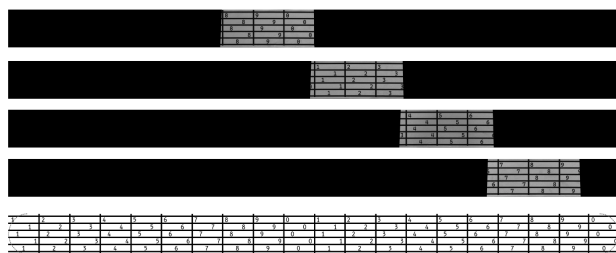


Figure 5: Perspective corrected images of the sub region within the field of view for each camera, with a technical drawing of the spectrometer screen target (bottom).

Image Recombination

By matching the size of the sub region images from each camera to the reference target, the images can be easily combined to create a single image of the target, representing the field of view of the entire camera array.

The four sub region images are overlaid by mapping them in-turn onto the reference target. Empty pixels are discarded, and any regions of overlap are accounted for by taking the average intensity value of the shared pixels.

Figure 6 shows the initial recombination result from overlaying two neighbouring camera images with this method. Whilst the geometric features of the target are successfully matched, it is clear this recombination suffers from vignetting effects.

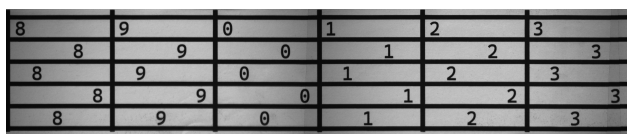


Figure 6: Two adjacent sub regions of the screen target overlaid for image recombination. Due to vignetting, the distinct images and seams are apparent.

By imaging an approximately uniform light source through one of the array cameras and the 75 mm lens, a calibration image is obtained, essentially creating a vignetting map. By dividing the screen target images by the normalised vignetting map, the variations in brightness across the target images are compensated.

Figure 7 is the result of complete image recombination of the four spectrometer cameras, correcting for vignetting, lens and perspective distortion.



Figure 7: All four spectrometer camera images combined into a single image of the screen target.

The leading advantage to this image recombination technique is the lack of constraint around overlap between cameras in the array. If images were combined via an image stitching method, this would require a sufficient overlap between neighbouring cameras, ensuring an adequate number

of common descriptors could be identified. This constraint reduces the maximum field of view achievable compared to recombination by image overlaying for a camera array of a given size.

Resolution

It is worth noting that the lens distortion and perspective corrections performed in this work change the underlying pixel grid of the images, and are therefore interpolations. For this reason, it is important to assess the resolution both prior to and after these corrections. The reference image is sampled upwards, creating a reference with substantially more pixels than the images from the camera array. This reduces any loss of information during the perspective correction from the original image grid to the reference.

The image resolution is measured by imaging a resolution target and calculating the Modulation Transfer Function (MTF). In the case of the resolution targets in Fig. 4, the 0.5 MTF value before correction is ~3.9 line pairs per mm. After distortion and perspective correcting the image, the 0.5 MTF value is calculated as ~3.8 line pairs per mm. This shows a negligible change in the overall resolution due to image processing. It therefore remains advantageous to correct for the lens and perspective distortions prior to emittance analysis.

CONCLUSIONS

The AWAKE experiment continues studying the plasma acceleration of electrons in a wakefield generated by a proton bunch. To allow the measurement of the accelerated electron beam, improvements in the spectrometer system are required. This work discusses the improvements of the spectrometer optical system, with the aim of high-resolution imaging of the 1 m-long scintillator. The use of a camera array is proposed, and the hardware selection is presented. The image processing algorithm to recombine the single camera images into the full scintillator image is described, as well as the impact on the overall resolution of the process.

ACKNOWLEDGEMENTS

The authors would like to thank Mr. Itaru Sakamoto and the Mitsubishi Chemical Corp. for kindly providing the test scintillator samples. The authors would like to acknowledge the SPS and AWAKE operation teams, M. Gasior and T. Levens for the ICT support and S. Burger for the stimulating discussions.

REFERENCES

- [1] E. Adli *et al.*, “Acceleration of electrons in the plasma wakefield of a proton bunch,” *Nature*, vol. 561, no. 7723, pp. 363–367, 2018. doi:10.1038/s41586-018-0485-4
- [2] L. C. Deacon *et al.*, “Development of a Spectrometer for Proton Driven Plasma Wakefield Accelerated Electrons at AWAKE,” in *Proc. IPAC’15*, Richmond, VA, USA, May 2015, pp. 2601–2604. doi:10.18429/JACoW-IPAC2015-WEPWA045

- [3] L. C. Deacon *et al.*, “A Spectrometer for Proton Driven Plasma Accelerated Electrons at AWAKE - Recent Developments,” in *Proc. IPAC’16*, Busan, Korea, May 2016, pp. 2605–2608.
doi:10.18429/JACoW-IPAC2016-WEPMY024
- [4] F. Keeble *et al.*, “The AWAKE Electron Spectrometer,” in *Proc. IPAC’18*, Vancouver, Canada, Apr.-May 2018, pp. 4947–4950.
doi:10.18429/JACoW-IPAC2018-THPML118
- [5] J. Bauche *et al.*, “A magnetic spectrometer to measure electron bunches accelerated at AWAKE,” *Nucl. Instrum. Methods Phys. Res., Sect. A*, vol. 940, pp. 103–108, 2019.
doi:10.1016/j.nima.2019.05.067
- [6] F. Keeble, “Measurement of the electron energy distribution at awake,” Ph.D. dissertation, University College London, 2019.
- [7] D. A. Cooke *et al.*, “Measurement and application of electron stripping of ultrarelativistic $^{208}\text{Pb}^{81+}$,” *Nucl. Instrum. Methods Phys. Res., Sect. A*, vol. 988, p. 164902, 2021.
doi:10.1016/j.nima.2020.164902
- [8] D. A. Cooke *et al.*, “Calibration of the AWAKE Electron Spectrometer with Electrons Derived from a Partially Stripped Ion Beam,” in *Proc. IPAC’19*, Melbourne, Australia, May 2019, pp. 2694–2696.
doi:10.18429/JACoW-IPAC2019-WEPGW089
- [9] S. Mazzoni *et al.*, “Beam Instrumentation Developments for the Advanced Proton Driven Plasma Wakefield Acceleration Experiment at CERN,” in *Proc. IPAC’17*, Copenhagen, Denmark, May 2017, pp. 404–407.
doi:10.18429/JACoW-IPAC2017-MOPAB119
- [10] I. Gorgisyan *et al.*, “Commissioning of Beam Instrumentation at the CERN AWAKE Facility After Integration of the Electron Beam Line,” in *Proc. IPAC’18*, Vancouver, Canada, Apr.-May 2018, pp. 1993–1996.
doi:10.18429/JACoW-IPAC2018-WEPAF070
- [11] D. Gamba *et al.*, “The CLEAR user facility at CERN,” *Nucl. Instrum. Methods Phys. Res., Sect. A*, vol. 909, pp. 480–483, 2018, 3rd European Advanced Accelerator Concepts workshop (EAAC2017).
doi:10.1016/j.nima.2017.11.080
- [12] Bergoz Instrumentation. <https://www.bergoz.com/>
- [13] E. Senes *et al.*, “Recent AWAKE Diagnostics Development and Operational Results,” no. 13, pp. 343–346, 2022.
doi:10.18429/JACoW-IPAC2022-MOPOPT042
- [14] Z. Zhang, “A flexible new technique for camera calibration,” *IEEE Trans. Pattern Anal. Mach. Intell.*, vol. 22, no. 11, pp. 1330–1334, 2000. doi:10.1109/34.888718
- [15] G. Bradski, “The openCV library,” *Dr. Dobb’s Journal: Software Tools for the Professional Programmer*, vol. 25, no. 11, pp. 120–123, 2000.
- [16] P. Ram and S. Padmavathi, “Analysis of harris corner detection for color images,” in *2016 International Conference on Signal Processing, Communication, Power and Embedded System (SCOPEs)*, 2016, pp. 405–410.
doi:10.1109/SCOPEs.2016.7955862